Contents lists available at ScienceDirect

Biomaterials

journal homepage: www.elsevier.com/locate/biomaterials



Magnesium alloy based interference screw developed for ACL reconstruction attenuates peri-tunnel bone loss in rabbits



Jiali Wang ^{a, 1}, Yuanhao Wu ^{b, 1}, Huafang Li ^{a, 1}, Yang Liu ^c, Xueling Bai ^d, Wingho Chau ^a, Yufeng Zheng ^{b, c, **}, Ling Qin ^{a, d, *}

- a Musculoskeletal Research Laboratory of Department of Orthopaedics & Traumatology and Innovative Orthopaedic Biomaterial and Drug Translational Research Laboratory of Li Ka Shing Institute of Health Sciences, The Chinese University of Hong Kong, Hong Kong, China
- Center for Biomedical Materials and Tissue Engineering, Academy for Advanced Interdisciplinary Studies, Peking University, Beijing 100871, China
- c State Key Laboratory for Turbulence and Complex System and Department of Materials Science and Engineering, College of Engineering, Peking University, Beijing 100871, PR China
- d Center for Translational Medicine Research and Development, Institute of Biomedical and Health Engineering, Chinese Academy of Sciences, Shenzhen 518055. China

ARTICLE INFO

Article history: Received 4 August 2017 Received in revised form 5 December 2017 Accepted 10 December 2017 Available online 11 December 2017

Kevwords: MgZnSr alloy ACL reconstruction Peri-tunnel bone loss Torsion test

ABSTRACT

Peri-tunnel bone loss after anterior cruciate ligament (ACL) reconstruction is often observed clinically, which may detrimentally affect tendon graft integration with surrounding bone tissue. Biodegradable magnesium (Mg) based fixators in terms of interference screws may be suitable for fixation of the tendon graft due to their favorable effects on promotion of new bone formation. However, the poor mechanical strength of Mg is still one of the major challenges for its clinical applications. The addition of alloying elements into Mg is one of the strategies to improve their mechanical properties. Here, we prepared magnesium (Mg)-(4 and 6 wt%) zinc (Zn)-(0.2, 0.5, 1 and 2 wt%) strontium(Sr) alloys and tested their potential for attenuating peri-tunnel bone loss in ACL reconstruction. The optimal (6 wt%) Zn and (0.5 wt %) Sr contents were screened with respect to the microstructures, mechanical properties and corrosion behavior of these alloys. As compared to pure Mg, Mg-6Zn-0.5Sr rods and screws showed significantly higher torque and torsional stiffness in both numerical and experimental analysis. The in vitro cytocompatibility of Mg-6Zn-0.5Sr alloy was assessed with MTT test and fluorescence assay. The Mg-6Zn-0.5Sr interference screw was designed for fixation of the tendon graft to the femoral tunnel in a rabbit model of ACL reconstruction, with a commercially available poly-lactide (PLA) screw for comparison. In vivo high resolution peripheral quantitative computed tomography (HR-pQCT) scanning was performed to measure the degradation behavior of Mg-6Zn-0.5Sr interference screws and peri-tunnel bone quality at 0, 6, 12 and 16 weeks post-surgically. Mg-6Zn-0.5Sr interference screw was completely degraded within 12 weeks after surgery. The peri-tunnel bone loss was significantly attenuated in the Mg-6Zn-0.5Sr group when compared to the PLA group. Importantly, the bony ingrowth rapidly filled the cavity left by the complete degradation of Mg-6Zn-0.5Sr screws at 16 weeks. In histological analysis, more bone formation was observed in peri-tunnel region in the Mg-6Zn-0.5Sr group in comparison to the PLA group at 6 and 16 weeks after surgery. The femur-tendon graft-tibia complex was harvested at the end of week 6 and 16 post-operation for tensile testing. The maximum load to failure was significantly improved in the Mg-6Zn-0.5Sr group at week 16 post-operation. Therefore, our results indicate the potential clinical application of MgZnSr based interference screws in ACL reconstruction.

© 2017 Published by Elsevier Ltd.

1. Introduction

Anterior cruciate ligament (ACL) tear is one of the most common types of knee injuries and may subsequently lead to a higher risk of developing knee osteoarthritis (OA) in patients due to the loss of knee stability if no clinical treatment is performed [1,2]. In cases of ACL rupture, the patients may have to require ACL reconstruction

^{*} Corresponding author, Musculoskeletal Research Laboratory of Department of Orthopaedics & Traumatology and Innovative Orthopaedic Biomaterial and Drug Translational Research Laboratory of Li Ka Shing Institute of Health Sciences, The Chinese University of Hong Kong, Hong Kong, China.

^{**} Corresponding author. Center for Biomedical Materials and Tissue Engineering, Academy for Advanced Interdisciplinary Studies, Peking University, Beijing 100871,

E-mail addresses: yfzheng@pku.edu.cn (Y. Zheng), qin@ort.cuhk.edu.hk (L. Qin).

¹ These authors contributed equally to this work.

(ACLR) surgery to restore their knee function and prevent OA and its progression [3,4]. Although most of patients can return to sports after surgery, there is still about 25% failure rate in clinical outcomes [5], which may be ascribed to traumatic, technical, infection, and biologic factors [6]. In addition to these causes, peri-tunnel bone loss, which is often observed in clinical studies, may result in less bone around for tendon graft integration and subsequently impair the tendon graft-bone junction healing [7]. Hence, the reduction of bone loss around tunnels is one of strategies to promote the graft healing.

More and more researchers and surgeons have shown increasing interests in the Research & Development (R&D) of Mg or its alloys based implants due to their excellent biocompatibility, degradation and osteopromotive properties [8–13]. Till now, a series of novel Mg based alloys, which possess improved corrosion resistance or higher mechanical strength, have been developed as potential orthopaedic devices in different animal models to mimic relevant clinical indications for both biosafety and bio-efficacy assessment [14–18]. In addition, extensive work has also been performed on how to propose a reliable in vitro model with relevant factors influencing corrosion performance of Mg metals, for more precise pre-screening information of in vivo degradation behavior of potential Mg based devices, which has greatly accelerated the R&D of novel Mg based implants [19,20]. The released Mg ions, which are accompanied by the degradation of Mg implants, have been reported to enhance osteogenic activity of mesenchymal stem cells (MSCs) [21], so the high-purity Mg interference screws have been recently developed for fixation of the tendon graft in animals underwent ACLR with encouraging results [22-25]. Indeed, highpurity Mg has close elastic modulus to the cortical bone [26], which can mitigate the stress shielding effects to facilitate new bone formation. However, the ultimate mechanical strength of the high-purity Mg fixators is still not sufficient to bear the load at weight-bearing skeletal sites and even during the surgery, for example during screw tightening (Supplementary Fig. 1), which is one of the most challenging issues that prevents clinical applications of pure Mg implants [27]. The addition of alloying elements which are soluble in Mg has been widely considered as one of effective strategies to improve the mechanical strength of Mg based materials [28]. Although, AZ31 (aluminum 3 wt% and zinc 1 wt%) interference screws have been previously reported to restore the knee stability and graft function of goats without observation of any adverse effects [29], the addition of aluminum into the Mg based implants is still a serious clinical concern on inducing potential neuronal injury. Among the candidates of alloying elements with low toxicity, Zinc (Zn) is an important element with a relatively high solubility in Mg and also is able to enhance mechanical properties of the alloy because of its solid solution strengthening and aging strengthening effects [28]. The zinc distribution in the α -Mg phase is not uniformly distributed in Mg-Zn alloys with Zn concentrations higher than 6% (the maximal solid solubility), otherwise the precipitation of Mg-Zn phase will be formed at the dendrite edges, which will ultimately impair the corrosion resistance of Mg-Zn alloys [28]. Taking both mechanical properties and corrosion resistance as main concerns, the preparation of ternary alloys may open up a new path for the R&D of orthopaedic devices attributed to their combined effects of alloying elements on the microstructure of the alloys. Strontium (Sr) and calcium (Ca), belongs to the same group of Mg in the periodic table and shares similar chemical and metallurgical properties [30]. Low contents of Ca and Sr were found to slow down the degradation rate [28]. From the viewpoint of biological effects, Ca ions compete with Mg ions for binding sites, leading to lower influx of Mg ions into cells for biological reactions [31]. Consequently, Sr, which is an osteopromotive mineral element [32], is more suitable as a third alloying element in Mg-Zn alloys.

In this study, we prepared a series of Mg-Zn-Sr ternary alloys for screening one of available candidates with superior mechanical strength and osteopromotive properties for *in vivo* testing using experimental ACLR model, especially with focus on prevention of postoperative peri-tunnel bone loss.

2. Materials and methods

2.1. Alloys preparation

The alloys developed for the present study were as-extruded Mg-(4, 6 wt%)Zn-(0.2, 0.5, 1, 2 wt%)Sr ternary. Pure Mg (99.9 wt %), Zn (99.9 wt%) and Sr (99.9 wt%) ingots were selected as raw materials. The Mg-Zn-Sr ternary alloys ingots were prepared by permanent mold casting at a pouring temperature of 720 °C and air cooling. The as-cast billets of the alloys were solution treated at 340 °C for about 4 h and then guenched in water. Finally, the solution treated alloy samples were hot extruded directly into bars at 320 °C with an extrusion speed and extrusion ratio of 20 mm/min and 12, respectively. Disk alloy samples with a diameter of 12 mm and a height of 2 mm were directly cut from the as-extruded bars. All the disk sample surfaces were then mechanically ground on SiC abrasive papers up to 2000 grit. Subsequently, the ground disks were washed in acetone, absolute ethyl alcohol, deionized water and finally dried in air. The actual chemical composition of the ternary alloys, which was determined by using inductively coupled plasma atomic emission spectrometry (ICP-AES) (Leeman Labs, USA), is provided in Table 1.

2.2. Microstructure characterization

Prior to the microstructure characterization, the disk samples were etched with 4 vol% nitric acid distilled water solution. The microstructure of the Mg-Zn-Sr alloys was investigated by utilizing an optical microscope (Olympus BX51M, Japan). The phases of the as-extruded alloys were identified by an X-ray diffractometer (XRD) (Rigaku DMAX 2400, Japan) using a Cu $K\alpha$ radiation with a scanning angle from 10° to 90° and a scanning rate of 4°/min.

2.3. Tensile testing

The tensile property of the as-extruded alloys was measured at room temperature on a universal testing machine (INSTRON 5969, USA) with a crosshead speed about 1 mm/min. The specimens were cut into slices with an electrical discharge wire according to the ASTM-E8-04 standard from the extruded bars parallel to the extrusion direction [33]. Three parallel samples were used for each alloy.

2.4. Immersion test for morphological analysis of alloys

The immersion tests were carried out in Hank's solution with surface area to solution volume ratio of 1 cm²: 20 ml in accordance

 Table 1

 Nominal and actual composition of Mg-Zn-Sr ternary alloys.

Nominal Composition	Actual Composition (wt.%)						
	Zn	Sr	Si	Ni	Cu	Fe	Mg
Mg-4Zn-0,2Sr	3.82	0.24	0.053	< 0.001	0.0048	0.0032	Bal.
Mg-4Zn-0.5Sr	4.12	0.56	0.055	< 0.001	0.0034	0.0022	Bal.
Mg-4Zn-1Sr	4.14	1.20	0.061	< 0.001	0.0037	0.0033	Bal.
Mg-4Zn-2Sr	3.96	1.92	0.053	< 0.001	0.0038	0.0020	Bal.
Mg-6Zn-0.2Sr	5.88	0.19	0.044	< 0.001	0.0032	0.0025	Bal.
Mg-6Zn-0.5Sr	5.93	0.62	0.049	< 0.001	0.0038	0.0038	Bal.
Mg-6Zn-1Sr	5.89	1.08	0.053	< 0.001	0.0028	0.0024	Bal.
Mg-6Zn-2Sr	6.21	2.15	0.042	< 0.001	0.0052	0.0036	Bal.

with ASTM-G31-72 [34]. In order to avoid evaporation of the Hank's solution, the tubes were all sealed during the immersion period and the temperature of the immersion medium was kept at 37 °C with water bath. The alloy samples were removed after 3 days' immersion, gently rinsed with distilled water and dried at room temperature. The surface morphology of the alloys after immersed was characterized by environmental scanning electronic microscopy (SEM) (FEI Quanta 200 FEG, USA).

2.5. Measurement of in vitro degradation of alloys

The hydrogen evolution volume and degradation rate of MgZnSr ternary alloys were detected by volumetric measurements. Three samples prepared in cylindrical disk were immersed in Hank's solution with surface area to Hank's solution volume ratio of 1 cm²: 40 ml. Hydrogen evolution volume was detected every 4 h in the first two days, and then detected every 12 h.

In addition, electrochemical test was applied using Metrohm Auto workstation (Metrohm Autolab, Netherland) in a standard three-electrode cell in a beaker containing 250 ml Hank's solution. The alloy disks were used as working electrode with 0.20 cm² of exposed area. A platinum electrode was worked as counter electrode and a saturated calomel electrode (SCE) was worked as reference electrode. The polarization curves were used to estimate the corrosion current density (i_{corr}) and corrosion potential (E_{corr}) by Tafel extrapolation methods.

2.6. Numerical stimulation of torsion test in screw

To gain the understanding on the distribution of the strains and stresses occurring in the screw's complex geometry during the torsion test, the experimental setup was reproduced virtually and analyzed by using the finite element analysis (FEA) method with ABAQUS software version 6.12 (Hibbit Inc., Rhode Island, USA). For achieving this aim, we created a mesh of tetrahedral elements within the 3D geometry of Mg-6Zn-0.5Sr and high-purity screw,

using plane elements to define the rigid surface of the screwdriver. The FE model consisted of two parts, i.e. the interference screw and the screw driver [35]. Quadratic tetrahedral elements of types were used in the model, in which 61982 elements were generated for the screw while 60 hexahedron elements were created for the screw driver. The screw driver was modelled as rigid and the interaction between the screw and the driver was set as frictionless contact. Fig. 1A shows the finite elements mesh for the screw. The tip of the screw (highlighted area in Fig. 1B) was clamped while a controlled rotation at 0.02 radian/s (Fig. 1C) was prescribed for the screw driver. To model the mechanical response of Mg and Mg-6Zn-0.5Sr screws, an elastoplastic constitutive model was used. In this model, yield strength $\sigma_v = 117$ MPa, Young's modulus E = 45.3 GPa and Poisson ratiov = 0.30 was used for Mg-6Zn-0.5Sr screw while $\sigma_v = 24$ MPa, E = 44.8 GPa and v = 0.35 was applied for high purity Mg screw according to our obtained data. The Equivalent plastic strain and Maximum principal stress in the screw were examined.

2.7. Torsion test of rods

The torsion test was carried out on Mg-6Zn-0.5Sr rods with a dimension of $\phi 10~mm \times 125~mm$ at a constant rate of 0.25 rpm in a torsion test machine (INSTRON E1000, USA) according to ISO 7800-2012 standards [36]. High purity Mg (99.99 wt%) rods with the same size was prepared as the control. The torque (Nm) versus twist angle (deg) was recorded for the calculation of maximal torque (Nm). Six samples were used for each group.

2.8. Cyto-compatibility test

Mg-6Zn-0.5Sr specimens were immersed into Dulbecco's modified eagle medium (DMEM, Invitrogen, USA) supplemented with 10% fetal bovine serum (Gibco, Thermo Scientific, USA) for 72 h under cell culture conditions (5% CO₂, 95% humidity, 37 °C) with a fixed mass ratio to medium volume (0.2 g/ml) for preparing extracts according to ISO 10993-12 [37]. The ion concentrations of

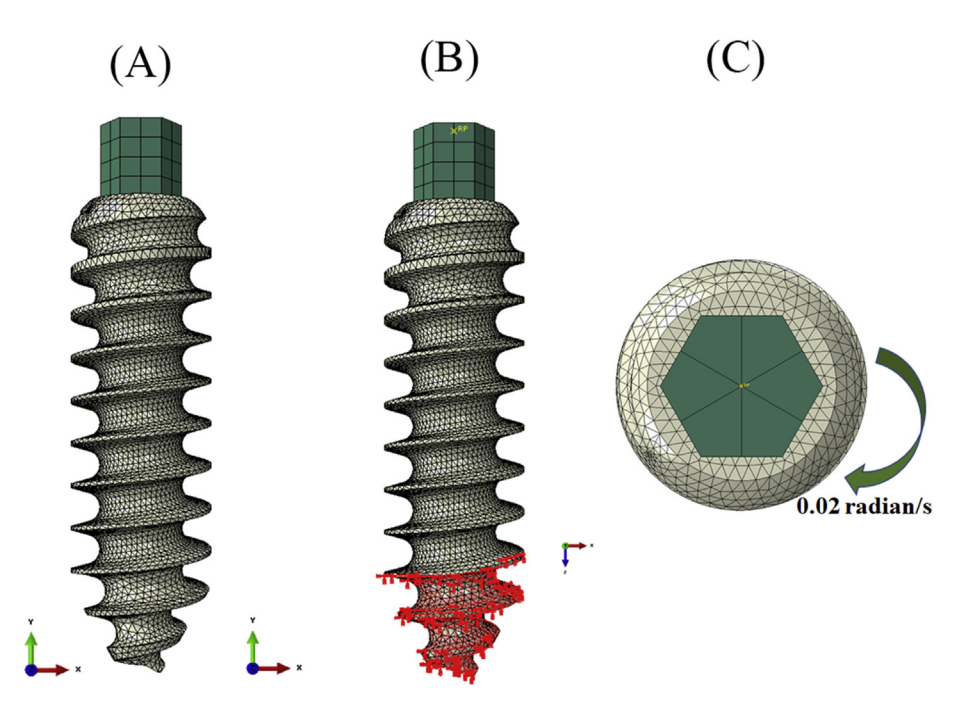


Fig. 1. The proposed finite elements model for the screw tightening. (A) Images of finite elements mesh for the screw and driver. (B) The boundary condition set for the analysis. The screw tip (highlighted area in red) was fixed when a rotation was applied. (C) A controlled rotation rate of 0.02 radian/s in clockwise direction was prescribed for the screw driver. (For interpretation of the references to colour in this figure legend, the reader is referred to the Web version of this article.)

Mg, Zn and Sr in the extracts were measured by ICP-AES (Leeman Labs, USA). The original extract is called $1\times$. The extract was then diluted with fresh cell culture medium for 3 and 6 times (called $3\times$ and $6\times$, respectively). Bone marrow stem cells (BMSCs) isolated from rats at passage 3 were cultured in these extracts for 24 h and 48 h, respectively, according to our previous protocol [38]. Cell viability was evaluated using both 3-(4,5-Dimethylthiazol-2-yl)-2,5-Diphenyltetrazolium Bromide (MTT) and live/dead fluorescence assays following manufacturer's protocol.

2.9. Animal surgery

The Mg-6Zn-0.5Sr rods with 5 mm in diameter were used for the fabrication of specially designed hollow interference screw that was similar to commercially available screw for human applications [39]. Prior to animal surgery, the Mg-6Zn-0.5Sr screws were manufactured on a computerized numerically controlled lathe (SZ-20C, Sowin, Shenzhen, China). All screws were ultrasonically cleaned in absolute acetone and ethanol successively, followed by washing in distilled water prior to sterilization with 25 kGy of ⁶⁰Co radiation. The sterilized screws were then packaged in vaccum. The outer diameter and length of these screws were fixed as 3 and 8 mm, respectively, which was suitable for fixation of the tendon graft in rabbits. Details of Mg-6Zn-0.5Sr screws were listed in Supplementary Fig. 2. PLA screws with similar dimension parameters were purchased (Inion, Tampere, Finland). As shown in Supplementary Fig. 3, ACLR surgeries in skeletally matured male New Zealand White rabbits, which was approved by the Animal Experimentation Ethics Committee (AEEC) of the Chinese University of Hong Kong (AEEC No. 13-014/MIS-5), were performed according to our previously published protocol [40]. Briefly, under anesthesia, the long digital extensor tendon graft was harvested. Then, a medial parapatella arthrotomy was performed to expose the knee joint prior to patellar dislocation. The infrapatellar fat tissue was removed to expose the joint cavity for ACL transection. Afterwards, bone tunnels of 2.5 mm diameter were created in the femur and tibia through the footprint of the original ACL by using a bone drill via the transtibial technique to allow the placement of the harvested tendon graft. As the synovial fluid in the cavity of knee joint may result in fast degradation of Mg interference screw if the inside-out insertion direction is applied, which may ultimately cause the rapid loss of mechanical integrity in Mg screws, the outside-in screw insertion direction was applied in this study. Due to insufficient cancellous bone in the proximal tibia, the extraarticular graft fixation at the exit of the tibia was performed by using non-absorbable suture. Finally, the wound was sutured layer by layer. Both Mg-6Zn-0.5Sr and PLA interference screws were used in this study.

2.10. High resolution peripheral quantitative computed tomography (HR-pQCT) analysis

HR-pQCT (Scanco Medical AG, Switzerland) was used to monitor and quantify the degradation rates of Mg-6Zn-0.5Sr screws in peritunnel mass after surgery. 6 rabbits in each group (Mg-6Zn-0.5Sr and PLA) were used for *in vivo* CT scanning at defined postoperative time points during the entire experimental period. The rabbits were anesthetized for taking X-rays at week 0, 6, 12 and 16 after operation with a X ray-tube set at 60 kV, 1 mA and 82 μm in isotropic voxel size. The volume of the Mg-6Zn-0.5Sr screws were measured via 3D reconstruction of a series of 2D tomography images. In addition, the peri-tunnel bone tissue with an area of 0.0585 cm² was selected as region of interest (ROI) for 3D reconstruction based on a series of 2D tomography images. The resulting gray-images were segmented using a fixed threshold and a low-

pass filter to minimize the noise (Sigma = 1.2, support = 2.0, threshold = 145). Therefore, bone volume (BV), trabecular number (Tb.N), trabecular thickness (Tb.Th) and trabecular separation (Th.Sp) of peri-tunnel tissue were calculated.

2.11. Histological and histomorphological analysis

These animals were sacrificed at 6 and 16 weeks after surgery. To label newly formed bone, the fluorochrome calcein green (10 mg/kg) was intramuscularly injected into rabbits assigned for the two time points at 3 and 13 weeks post-surgically prior to xylenol orange (90 mg/kg) administration at 5 and 15 weeks postsurgically, respectively. Both decalcified and undecalcified samples at 6 and 16 weeks were used for histological examination. Briefly, all these harvested femoral samples were fixed in 4% neutral buffer formalin for 48 h and then embedded in paraffin or methylmethacrylate (MMA) according to our previously published protocols prior to tissue sectioning at mid-tunnel region for the following analysis [40]. Stevenel blue-Van Gieson-Alizarin Red S (SVA) staining was performed in MMA sections at a thickness of approximate 100 μ m [41]. Paraffin sections with 5 μ m in thickness were stained with hematoxylin and eosin (H&E). Six samples were used in each group at each postoperative time point.

2.12. Tensile testing of femur-tendon graft-tibia complexes

The femur-tendon graft-tibia complexes (FTGTC) at 6 and 16 weeks post-surgically were harvested and then stored in $-80\,^{\circ}$ C prior to biomechanical testing after thawing at room temperature. Except for the ACL graft, the suture on the tibial side and all the soft tissue were carefully removed while interference screws were kept in femoral tunnels prior to the fixation of femur and tibia with custom-designed jigs in a uniaxial mechanical testing machine (H25K-S, Hounsfield Test Equipment LTD, UK). The tensile tests were performed in FTGTC with the knee flexed to 90° with a preload of 1 N and a rate of 50 mm/min to record the maximal load to failure. Six samples were used for each group at each time point.

2.13. Statistical analysis

We used Student's t-test for comparisons between two groups and one-way ANOVA with Tukey's $post\ hoc$ test for multiple comparisons between two groups at various postoperative time points. All data were expressed as mean \pm standard deviation (SD) with the significant level set as p < .05 using SPSS 17.0 software (SPSS Inc. Chicago, IL).

3. Results

3.1. Alloy microstructure and mechanical properties

Fig. 2A shows the X-ray diffraction results of the as-extruded Mg-Zn-Sr ternary alloys. Fig. 2A-a: Mg₇Zn₃ phases were only detected in Mg-4Zn-0.5Sr alloy. The diffraction intensity of the MgZn second phases in Mg-4Zn-1Sr alloy were higher than that of Mg-4Zn-2Sr alloy, indicated that higher amounts MgZn phases in the Mg-4Zn-2Sr alloy. The intensity of Mg₁₇Sr₂ second phase was much higher than Mg-4Zn-2Sr alloy. Fig. 2A-b: Mg₁₇Sr₂ second phases were only detected in Mg-6Zn-0.2Sr alloy. Both the intensity of MgZn and Mg₇Zn₃ second phases were increased with Sr contents.

The microstructure of the Mg-Zn-Sr ternary alloys were shown in Fig. 2B. In the Mg-4Zn-(0.2, 0.5) Sr alloys, the second phase particles were mainly distributed in the grains. However, for the Mg-4Zn-(1, 2) Sr alloys, the second phases were mainly distributed

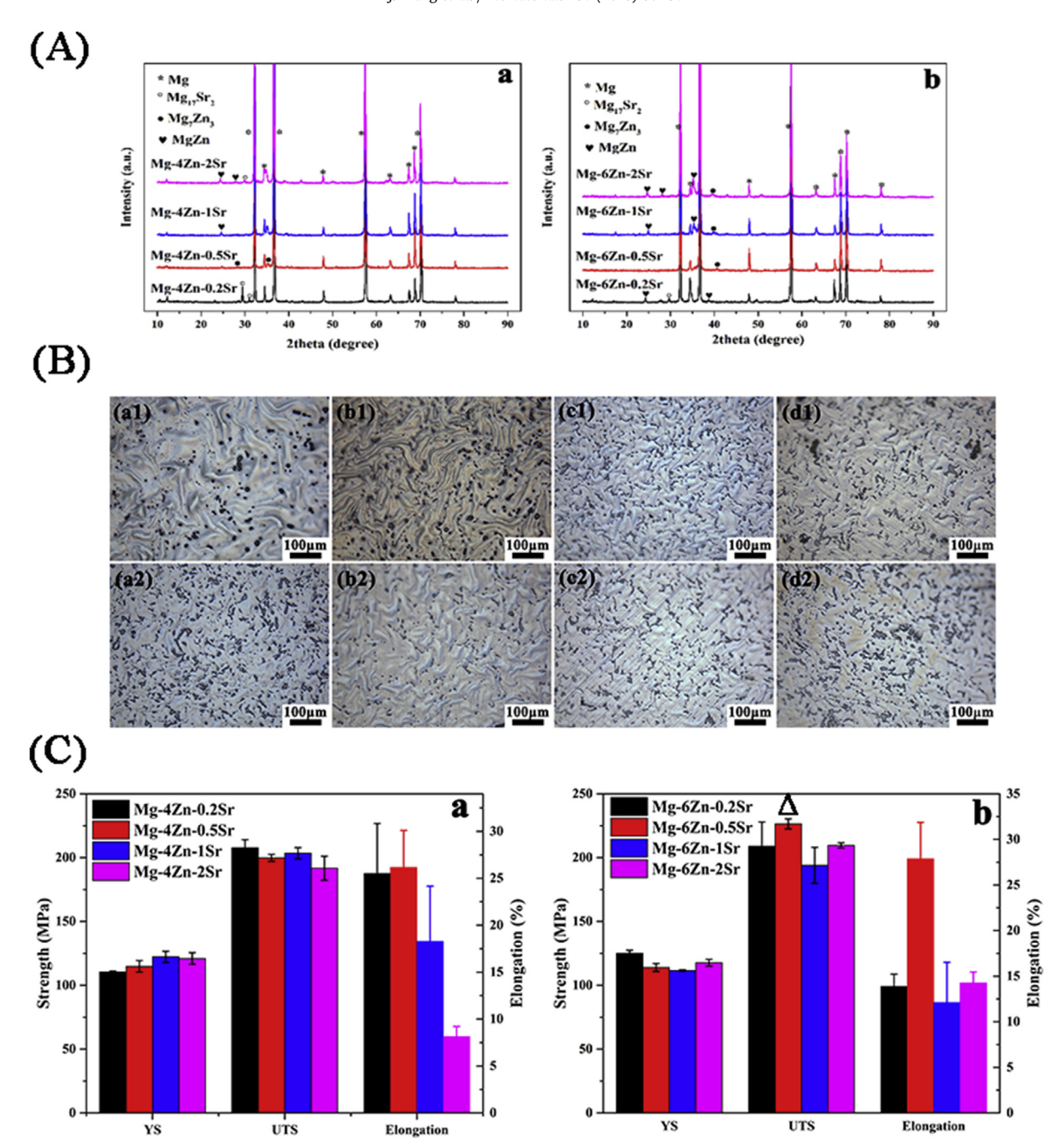


Fig. 2. Microstructure and mechanical properties of the as-extruded Mg-Zn-Sr ternary alloys. (A) X-ray diffraction results of Mg-4Zn-(0.2, 0.5, 1, 2)Sr alloys (a) and Mg-6Zn-(0.2, 0.5, 1, 2)Sr alloys (b). (B) Optical micrographs showing the microstructures of Mg-4Zn-0.2Sr (a1), Mg-4Zn-0.5Sr (b1), Mg-4Zn-1Sr (c1), Mg-4Zn-6Zn (d1), Mg-6Zn-0.2Sr (a2), Mg-6Zn-0.5Sr (b2), Mg-6Zn-1Sr (c2) and Mg-6Zn-2Sr (d2). (C) Yield strength, ultimate tensile strength and elongation of Mg-4Zn-(0.2, 0.5, 1, 2)Sr alloys (a) and Mg-6Zn-(0.2, 0.5, 1, 2) alloys (b) in tensile tests. Mg-6Zn-0.5Sr, which was indicated by the triangle, showed best mechanical properties among the ternary alloys.

in the grain boundaries. Courser grain boundaries can be seen in Mg-4Zn-2Sr alloy. For the alloys containing 6% Zn, the second phases were mainly distributed along the grain boundaries. Mg-6Zn-0.5Sr alloy exhibited much lower second phase contents than other 3 alloys.

Fig. 2C showed the mechanical properties of the as-extruded Mg-Zn-Sr ternary alloys. As we can see from Fig. 2C-a, the yield strength (YS) of Mg-4Zn-xSr ($x=0.2,\ 0.5,\ 1$ and 2) alloys was proportional to the Sr content with x lower than 2. Interestingly, when Sr content further increased up to 2%, the YS of Mg-4Zn-xSr alloys decreased. The ultimate tensile strength (UTS) showed little

fluctuation with different Sr contents and Mg-4Zn-0.2Sr alloy possess the highest UTS. The elongation rate of Mg-4Zn-xSr decreased when the addition of Sr was over 0.5%. In terms of Mg-6Zn-ySr ($y=0.2,\ 0.5,\ 1$ and 2) alloys shown in Fig. 2C-b, the YS decreased with higher Sr content when y was lower than 2. However, Mg-6Zn-0.5Sr exhibited highest UTS and elongation rate.

3.2. Corrosion behavior of alloys

The surface morphology of the as-extruded Mg-Zn-Sr alloys was depicted after immersed in Hank's solution for 3 days (Fig. 3A).

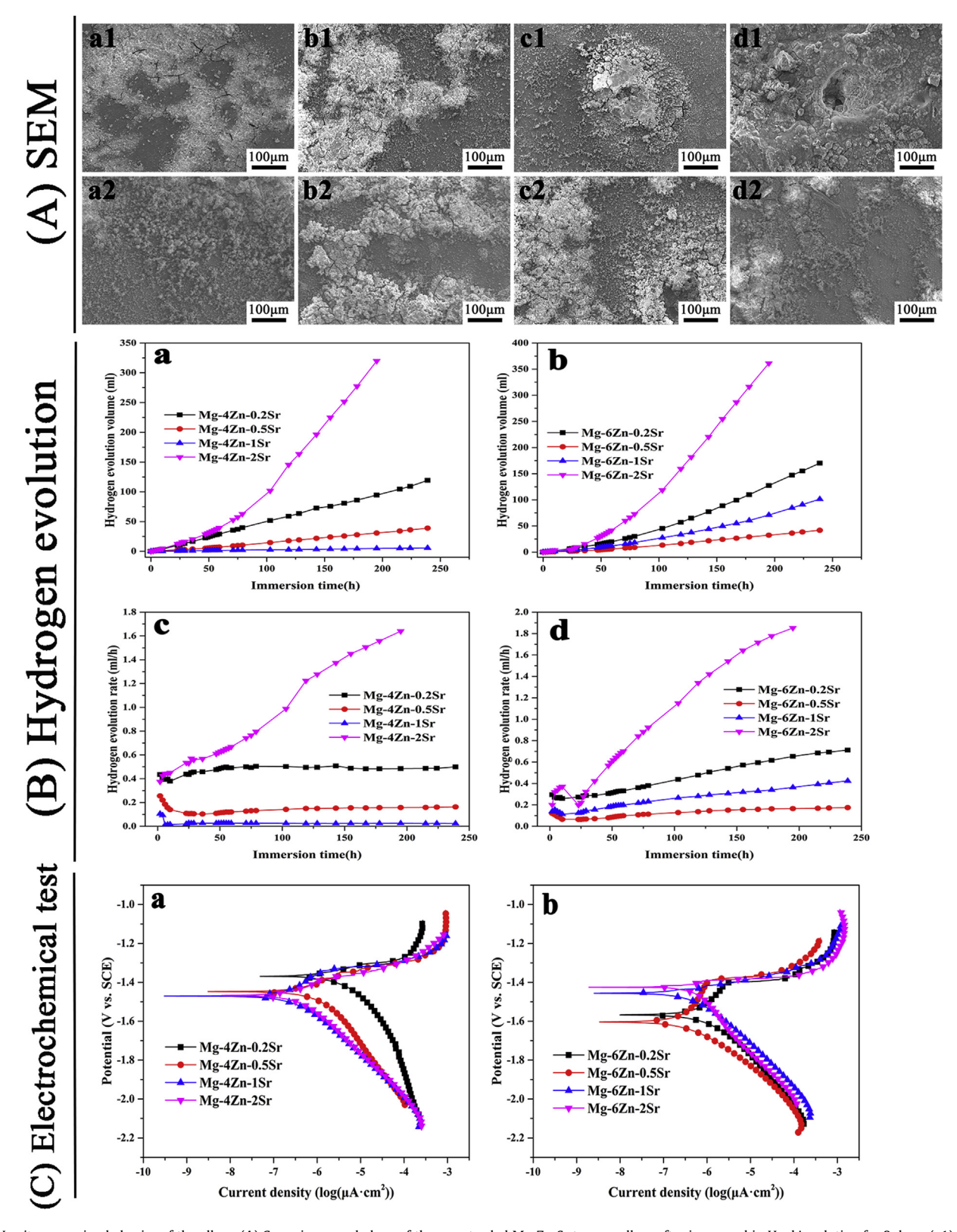


Fig. 3. *In vitro* corrosion behavior of the alloys. (A) Corrosion morphology of the as-extruded Mg-Zn-Sr ternary alloys after immersed in Hank's solution for 3 days: (a1) Mg-4Zn-0.2Sr; (b1) Mg-4Zn-0.5Sr; (c1) Mg-4Zn-0.5Sr; (c1) Mg-4Zn-0.5Sr; (c2) Mg-6Zn-0.5Sr; (c2) Mg-6Zn-1Sr; (d2) Mg-6Zn-2Sr. (B) Hydrogen evolution measurement. (a) and (b): hydrogen evolution volume; (c) and (d): hydrogen evolution rate. (C) Potentiodynamic polarization curves for the as-extruded Mg-Zn-Sr ternary measured in Hank's solution: (a) Mg-4Zn-(0.2, 0.5, 1, 2) Sr alloys; (b) Mg-6Zn-(0.2, 0.5, 1, 2) Sr alloys.

Many corrosion holes or cracks were observed in Mg-4Zn-2Sr and Mg-6Zn-2Sr alloys, indicating poor corrosion resistance for Mg-Zn-Sr ternary alloys with high Sr content. Hydrogen evolution and electrochemical measurements were performed for quantitative assessment of corrosion resistance of Mg-Zn-Sr alloys. As shown in Fig. 3B, Mg-4Zn-1Sr and Mg-6Zn-0.5Sr showed lowest hydrogen evolution rate during the entire immersion period in Mg-4Zn-xSr and Mg-6Zn-ySr ternary alloys (x, y = 0.2, 0.5, 1 and 2), respectively. The electrochemical results from the potentiodynamic polarization curves were supportive to above findings (Fig. 3C and Table 2).

3.3. Torsion test

Fig. 4A shows the distribution of equivalent accumulated plastic strains. The maximal values were observed near the head of both Mg and Mg-6Zn-0.5Sr screws. The distribution of the maximal principal stress was shown in Fig. 4B. Similarly, the highest stress concentrations were found near the screw head. Besides, it was found that much higher peak stress was obtained in Mg-6Zn-0.5Sr screw when compared to Mg screw. Mg-6Zn-0.5Sr screw showed

 Table 2

 Electrochemical corrosion data of as-extruded alloys in Hank's solution.

Sample	Corrosion Current Density	Corrosion Rate		
	(μA/cm ²)	(mm/year)		
Mgr-4Zn-0.2S	9.617 ± 1.909	0.220 ± 0.044		
Mg-4Zn-0.5Sr	5.858 ± 0.569	0.127 ± 0.013		
Mg-4Zn-1Sr	2.352 ± 1.013	0.054 ± 0.023		
Mg-4Zn-2Sr	7.036 ± 1.231	0.161 ± 0.028		
Mg-6Zn-0.2Sr	14.178 ± 0.852	0.325 ± 0.018		
Mg-6Zn-0.5Sr	2.980 ± 0.308	0.068 ± 0.007		
Mg-6Zn-1Sr	5.268 ± 0.192	0.119 ± 0.007		
Mg-6Zn-2Sr	14.461 ± 1.559	0.331 ± 0.036		

higher maximum torque angle than Mg screw. More importantly, the maximum torque in Mg-6Zn-0.5Sr screw is about 5-fold greater than that in Mg screw (Fig. 4C).

As shown in Fig. 5, Mg-6Zn-0.5Sr rods presented much higher maximum torque than high-purity Mg rods with the same dimension parameters at the same testing conditions (38.54 \pm 0.35 vs. 25.25 \pm 0.06 Nm, p < .01). Although the experimental data of both Mg-6Zn-0.5Sr and high-purity Mg interference screws was not tested, the experimental torque of Mg-6Zn-0.5Sr and high-purity Mg rods was principally consistent with the numerical findings, demonstrating a better material candidate for Mg-6Zn-0.5Sr metal as potential Mg based fixators in orthopaedic field.

3.4. Cyto-compatibility of Mg-6Zn-0.5Sr

The Mg, Zn and Sr concentrations of the extract of the Mg-6Zn-0.5Sr rods were shown in Fig. 6A. Cells with severe cytotoxicity

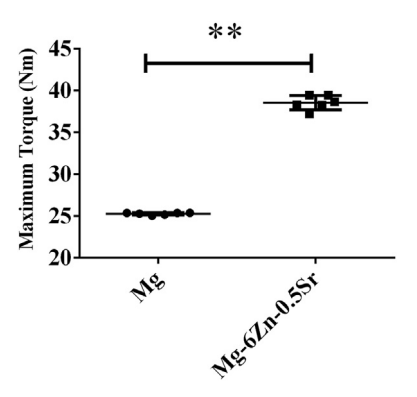


Fig. 5. Maximum torque of the high-purity Mg and Mg-6Zn-0.5Sr rods (10 mm in diameter) (n=6). Student's t-test, **p<.01.

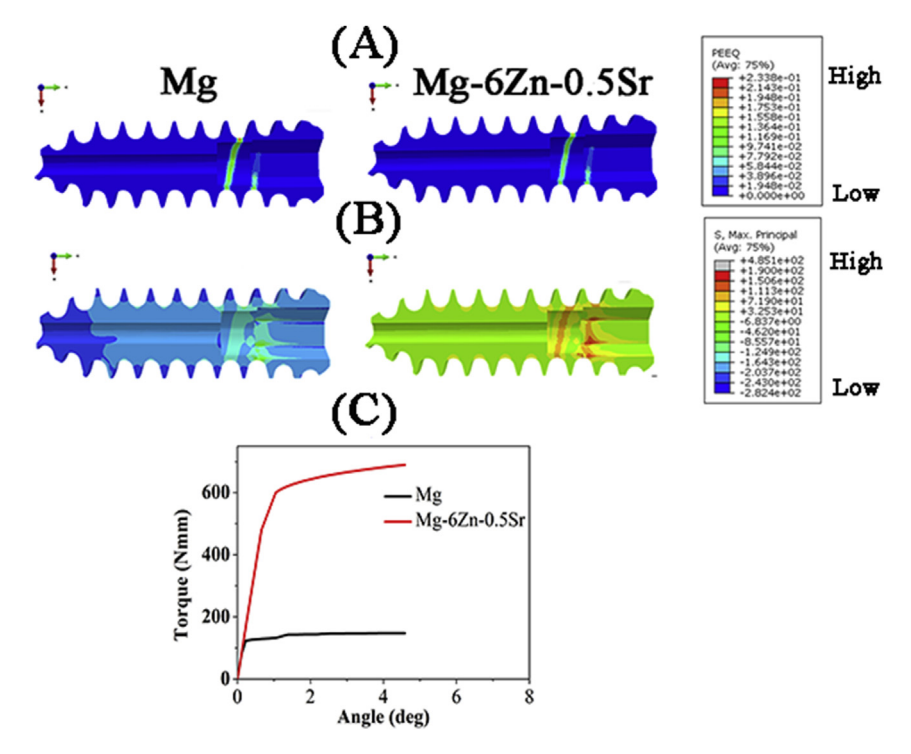


Fig. 4. Numerical stimulation of torsion test in Mg and Mg-6Zn-0.5Sr screws. (A) Equivalent accumulated plastic strains of Mg and Mg-6Zn-0.5Sr screws. (B) Maximum principal stress of Mg and Mg-6Zn-0.5Sr screws. (C) Curves on numerical torque versus angle for Mg and Mg-6Zn-0.5Sr screws.

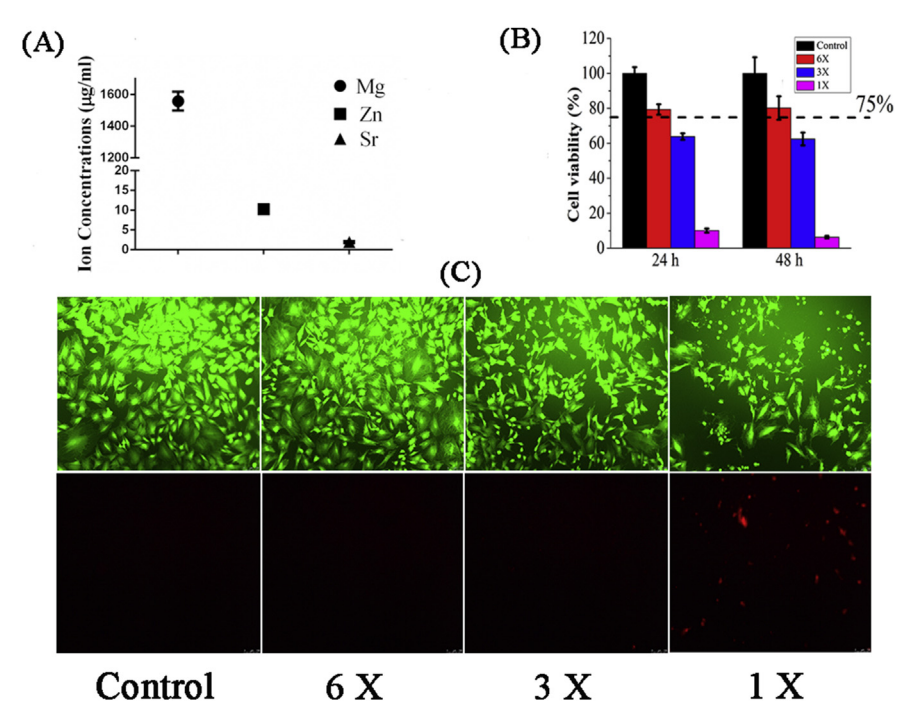


Fig. 6. Cyto-compatibility evaluation of Mg-6Zn-0.5Sr alloy. (A) Mg, Zn and Sr ion levels in the extract. (b) BMSCs viability test in the original extract and a series of diluted extracts. (C) representative fluorescent images for live (green)/dead (red) cell assay (100X). (For interpretation of the references to colour in this figure legend, the reader is referred to the Web version of this article.)

were detected in the original extract, whereas the extract diluted by 6 times led to non-cytotoxic results (Fig. 6B). Similarly, a large number of apoptotic cells and only a few live cells were observed in the original extract. However, the extract can remarkably improve the cell survival at a dilution of 6X (Fig. 6C).

3.5. HR-pQCT analysis of peri-tunnel bone mass and Mg-6Zn-0.5Sr screw degradation

The degradation rate of the Mg-6Zn-0.5Sr interference screws and the changes of the peri-tunnel bone mass in both Mg-6Zn-0.5Sr and PLA groups were shown in Fig. 7. The Mg-6Zn-0.5Sr screws showed a complete degradation within 16 weeks after surgery (Fig. 7A—C). The gas formation, which was accompanied by the degradation of the screws, was observed in the peri-implant tissue (Fig. 7B). The cavity left by the degradation of screws was then filled by the newly formed bone tissue at week 16 post-operation. More importantly, the degradation of Mg-6Zn-0.5Sr screws did not deteriorate peri-tunnel bone mass via measurement of BV, Tb.N, Tb.Th and Tb.Sp after surgical implantation, while the implantation of PLA screws significantly decreased BV, Tb.N and Tb.Th and increased Tb.Sp in peri-tunnel bone tissue within 16 weeks after surgery (Fig. 7D).

3.6. Histological analysis

As shown in Fig. 8, more bone was observed in the peri-tunnel region in the Mg-6Zn-0.5Sr group when compared to the PLA group at both 6 and 16 weeks post-operation according to histological sections stained with H&E and SVA, which were also supported by those with fluorescent labelling. The degradation products of the Mg-6Zn-0.5Sr screws induced the formation of the fibrous tissue around the screws at week 6 post-operation, which was not observable in the PLA group. Meanwhile, the gas voids in

the peri-screw tissue was observed in the Mg-6Zn-0.5Sr group. At week 16 post-operation, mature bone eventually replaced the fibrous tissue in the Mg-6Zn-0.5Sr group. The degradation of Mg-6Zn-0.5Sr screw was accompanied with the bony ingrowth, so the cavity left by the complete degradation of screws at week 16 post-operation was fully filled by the newly formed bone.

3.7. Tensile testing of femur-tendon graft-tibia complexes

There was no significant difference in the maximal load to failure between Mg-6Zn-0.5Sr group and PLA group at week 6 post-operation. However, the load to failure in Mg-6Zn-0.5Sr group was significantly higher than that in PLA group at week 16 post-operation (Fig. 9).

4. Discussion

In the present study, we developed a novel Mg alloy based interference screw with suitable dimension parameters for fixation of the tendon graft in ACL reconstruction without concerns about mechanical failure and peri-tunnel bone loss after surgery (Supplementary Fig. 4). The addition of Zn and Sr elements into Mg alloys can optimize their mechanical and corrosion properties [28]. In addition, Zn and Sr are known as osteopromotive elements for fabrication into potential medical devices or drugs [32,42], so we explored a series of Mg-xZn-ySr alloys (x = 4, 6 while y = 0.2, 0.5, 1, 2) in this study. Mg-6Zn-0.5Sr alloy showed best corrosion resistance and mechanical properties among these ternary alloys. Compared to previously used high purity Mg implant or screw [23], Mg-6Zn-0.5Sr sample had much higher maximum torque in both experimental and numerical torsion tests. Cytotoxicity test suggested that Mg-6Zn-0.5Sr alloy could be considered as a safe biomaterial for developing potential Class III medical devices according to our previously proposed guidelines [38]. Importantly,

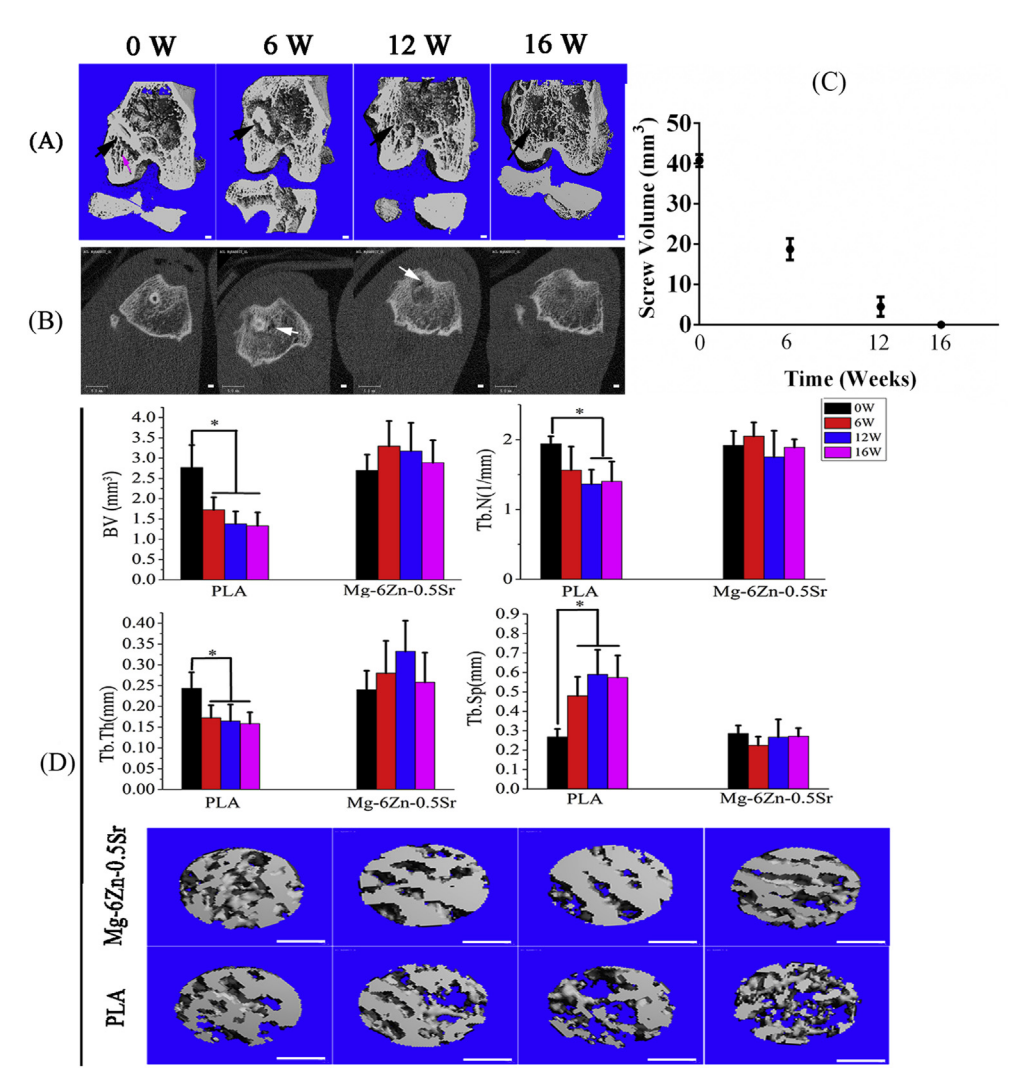


Fig. 7. HR-pQCT analysis of Mg-6Zn-0.5Sr interference screws and peri-tunnel bone mass. (A) The representative 3D reconstructed models of the femora in rabbits with ACL reconstruction. The screws and the targeted region of the peri-tunnel bone were indicated by the black and the pink arrows, respectively. (B) The representative 2D tomography images showing the gas (indicated by the white arrows) around the screws. (C) The volume changes of Mg-6Zn-0.5Sr screws in rabbits within 16 weeks after surgery (n = 4). (D) The peri-tunnel bone mass (BV, Tb.N, Tb.Th and Tb.Sp) in Mg-6Zn-0.5Sr and PLA groups within 16 weeks after operation (n = 6). One-way ANOVA with Tukey's *post hoc* test, *p < .05, Scale bar: 1 mm. (For interpretation of the references to colour in this figure legend, the reader is referred to the Web version of this article.)

the peri-tunnel bone loss was significantly attenuated in the Mg-6Zn-0.5Sr group when compared to the PLA group, resulting in a significantly higher load to failure in the Mg-6Zn-0.5Sr group at week 16 post-operation.

4.1. The optimal chemical composition of Mg-xZn-ySr ternary alloys

The incremental addition of Zn and Sr in the Mg-Zn-Sr ternary alloys lead to distinctive second phase composition and distribution. The Zn-containing second phases were Mg_7Zn_3 and MgZn phases while the Sr-containing second phase was $Mg_{17}Sr_2$, which are in agreement with the previous study for as-cast Mg-5Zn-Sr alloys [43]. The mechanical strength can benefit from the deposited second phases in the alloys by dispersion strengthening mechanism [44,45]. For Mg-4Zn-ySr ($y=0.2,\ 0.5,\ 1$ and 2) alloys, the second phase particles with round shape were mainly distributed in the grains for the Mg-4Zn-0.2Sr and Mg-4Zn-0.5Sr alloys. When Sr contents increased to 1 and 2%, more second phases were deposited along the grain boundaries. In terms of Mg-6Zn-ySr ($y=0.2,\ 0.5,\ 1$ and 2) alloys, the volume fraction of second phase in Mg-6Zn-0.5Sr alloy was much lower than other 3 alloys. As the

deposition of the hard brittle second phases around the grain boundaries can easily lead to intercrystalline brittle fracture in alloys in load-bearing conditions [28], the control of the second phases is critical for the development of Mg alloy based orthopaedic devices. Taking both tensile strength and elongation rate as the concerns, Mg-6Zn-0.5Sr alloys exhibited superior mechanical properties over other Mg-Zn-Sr ternary alloys.

The amounts of the deposited second phases also played a vital role in the corrosion behavior the Mg-Zn-Sr ternary alloys. It had been widely regarded that the second phase exhibited higher corrosion potential than α -Mg matrix, so small amounts of second phases may improve the corrosion resistance of the alloys. However, large volume fraction of the second phases would lead to the increased formation of galvanic corrosion couples between α -Mg matrix and the second phases and subsequently resulted in accelerated corrosion rate of the alloys. This may be the reason why Mg-4Zn-(0.5, 1)Sr and Mg-6Zn-(0.5, 1)Sr alloys showed relatively lower corrosion rate and hydrogen evolution volume. Taken together, Mg-6Zn-0.5Sr alloy has excellent mechanical properties and relatively lower corrosion rate, demonstrating a higher potential as medical devices over other Mg-Zn-Sr ternary alloys.

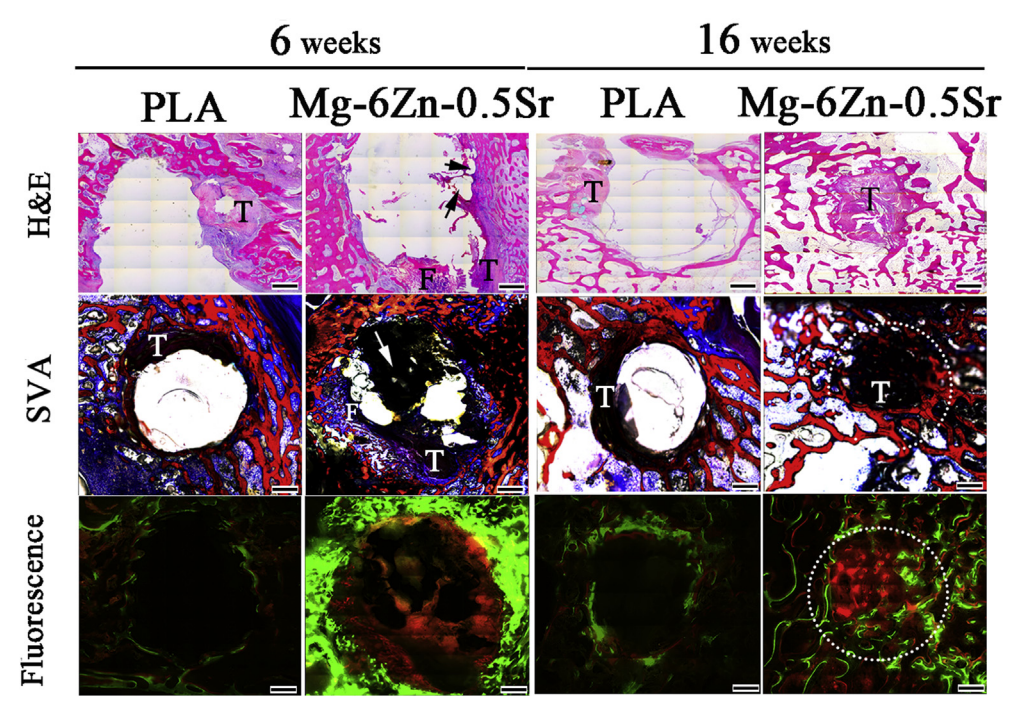


Fig. 8. Representative histology of the peri-tunnel tissue in the PLA and Mg-6Zn-0.5Sr groups at 6 and 16 weeks after surgery. F: fibrous tissue; T: tendon graft. Scar bar: 200 μm. The gas voids in surrounding tissue and the Mg-6Zn-0.5Sr were indicated by the black and the white arrows, respectively. The original bone tunnel was labelled by the white dotted circle.

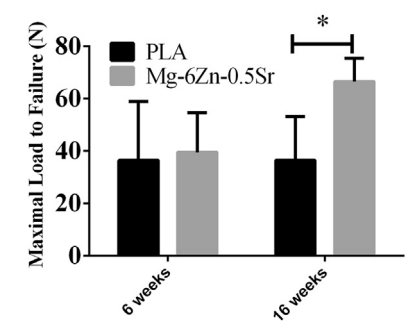


Fig. 9. Tensile property of femur-tendon graft-tibia complexes tested at week 6 and 16 post-operation after ACL reconstruction surgery in rabbits (n = 6). Student's t-test, ${}^*p < .05$.

4.2. The superior mechanical properties of Mg-6Zn-0.5Sr over high purity Mg as potential interference screws in ACL reconstruction

Although the use of high purity Mg interference screws has been reported to promote the osteointegration of the tendon graft into bone tunnels and inhibit graft degradation [22-24], it is still a serious clinical concern for the application of high purity Mg fixators in clinical trials due to their insufficient maximum torque (Supplementary Fig. 1). As the maximum torque of screw is proportional to the yield strength [46], the Mg-6Zn-0.5Sr based screw have higher maximum torque than high purity Mg screw, which then reduce the concern regarding the torque levels beyond the yield point during the insertion of screw into the bone. It is evident that the failure site after tensile test is near the screw head at rotation in both experimental and numerical torsion test, so the insertion of Mg screw into bone tunnels may cause the breakage in the screw head if the screw has low maximum torque. FEA, which has been widely applied in orthopaedic field for estimating the mechanical responses of medical devices to the applied external forces [47], provided a pre-screening information regarding maximum torque of Mg and Mg-6Zn-0.5Sr screws as potential fixators in ACL reconstruction. Much higher maximum principal stress was found distributed in the region of Mg-6Zn-0.5Sr screw head in comparison to that of high-purity Mg screw head, contributing to 5fold increase in maximum torque of Mg-6Zn-0.5Sr screw. Actually, the findings from the torsion test on rods were consistent with FEA results. Mg-6Zn-0.5Sr showed significantly higher maximum torque than high purity Mg rods, indicating a better material candidate for Mg-6Zn-0.5Sr fabricated into interference screws. Of note that we successfully inserted the whole body of Mg-6Zn-0.5Sr interference screw into bone tunnels without causing any breakage in screw head while the top portion of high purity screw was remained outside of bone tunnels due to the failure in screw head (Supplementary Fig. 1). As longer interference screws can provide better fixation ability in tendon graft [48], the use of Mg-6Zn-0.5Sr may fix tendon graft in bone tunnels more tightly in the initial healing stage, which is crucial for the graft healing prior to stable interzone structure formed at the tendon-bone interface [49].

4.3. The effects of Mg-6Zn-0.5Sr screws on peri-tunnel bone tissue in animals after ACL reconstruction

The peri-tunnel bone loss usually occurs in the early time post ACL reconstruction operation, which may be ascribed to high expression of matrix metallopeptidase 1 (MMP1), MMP13 and CD68+ cells at the tendon-bone surface and peri-tunnel tissue [50], may pose potential micro fracture of surrounding trabecular bone due to reduced bone strength and subsequently affect the graft osteointegration [51]. Although Mg-based implants have been increasingly reported to enhance bone formation and decrease MMP13 expression levels as potential orthopaedic devices [12,22], the use of high purity Mg interference screw did not effectively attenuate peri-tunnel bone mass according to our previous studies [23]. We found that Mg ions could not only positively

promote osteoblastgenesis, but also increase osteoclastogensis (Supplementary Fig. 5), which was consistent with Wu's findings on enhanced local bone turnover [52]. As Sr can enhance new bone formation by activating Wnt/Catenin signaling while decrease bone resorption [32,53], the addition of Sr into Mg alloys for fabrication into medical devices may be a potential strategy to increase bone mass. In addition, our previous studies showed that Zn based implants have shown beneficial effects on new bone formation [54]. It has been reported that the addition of Zn into Mg matrix may behave synergic effects on osteogenic differentiation of MSCs attributed to the anabolic role of Zn ions in ZIP1 (a ubiquitous zinc transporter for zinc influx) and inhibitive role of Mg ions in ZnT1 (zinc exporters) [55]. Therefore, the degradation of Mg-Zn-Sr alloy based interference screw may potentially reduce peri-tunnel bone loss. Compared to the PLA group, Mg-6Zn-0.5Sr screw effectively attenuated peri-tunnel bone loss as demonstrated by HR-pQCT based bone histomorphometry (BV, Tb.N, Tb.Th and Tb.Sp values). In histology, more trabecular bone around bone tunnels was observed in the Mg-6Zn-0.5Sr group with comparison to the PLA group. The released ions from Mg-6Zn-0.5Sr screw resulted in larger fluorescent positive area in surrounding bone tissue around tunnels, indicating promoted new bone formation. More trabecular bone around bone tunnels can minimize bone fracture in tunnel surface and maintain the fixation strength of the tendon graft into tunnels for better healing. Therefore, we observed a significant increase in the maximal load to failure of FTGTC in the Mg-6Zn-0.5Sr group when compared to the PLA group at week 16 postoperation, indicating the beneficial effects of Mg-6Zn-0.5Sr metals on the graft healing. Although the released metal ions from the Mg-6Zn-0.5Sr screws can contribute to the graft healing, the production of the gas accompanied with the degradation of the Mg-6Zn-0.5Sr screws may deteriorate the surrounding tissue via the formation and accumulation of gas voids. Interestingly, although the Mg-6Zn-0.5Sr screws showed a relatively fast degradation rate within the graft healing period, we did not observe the accumulation of a large amount of gas in the peri-implant tissue both radiographically and histologically, which might be ascribed to the buffering role of the knee joint space for the diffusion and excretion of the gas in the local tissue [56].

There are some limitations in this study. Although rabbit is the most frequently used animal model to mimic patients underwent ACL reconstruction (Supplementary Fig. 6), we still need to perform more studies in larger animals such as sheep and goats for bioefficacy assessment. The use of the larger animals indicates higher demands on animal holding and testing with significant high costs, but they move via walking rather than hopping, which may provide more precise pre-screening information for the clinical trials. As the goat has the most similar anatomy to the human knee, we will select goat as the animal model to conduct ACL reconstruction for the next stage prior to clinical trial application [57]. In addition, in terms of the R&D of available Mg based interference screws for clinical use, it is still necessary to improve the corrosion resistance of currently used Mg-6Zn-0.5Sr. Micro-arc oxidation (MAO) treatment will be adopted to control the degradation rate of Mg-6Zn-0.5Sr screws in our future studies [58].

5. Conclusion

This study developed and tested a series of Mg-(4 and 6 wt%) Zn-(0.2, 0.5, 1 and 2 wt%) Sr alloys as potential biodegradable fixators for ACL reconstruction. Mg-6Zn-0.5Sr showed superior mechanical properties and corrosion resistance over other formulations or alloys. Mg-6Zn-0.5Sr has significant superior maximum torque than that of high purity Mg in both experimental and numerical torsion tests. Compared to traditional degradable PLA

group, Mg-6Zn-0.5Sr interference screw significantly increased peri-tunnel bone mass in rabbits after ACL reconstruction within 16 weeks both radiographically and histologically, which ultimately contributed to a significant increase in the maximal load to failure for FTGTC in the Mg-6Zn-0.5Sr group with comparison to the PLA group. In conclusion, the use of Mg-6Zn-0.5Sr interference screws could provide sufficient mechanical strength to fix the tendon graft during the entire graft healing period and effectively attenuate the peri-tunnel bone loss as potential fixators in ACL reconstruction.

Acknowledgements

This work was supported by the NSFC/RGC Joint Research Scheme with the Grant No. 51361165101 in Mainland China and N_CUHK449/13 in Hong Kong and partially supported by a grant from the Research Grants Council of the Hong Kong Special Administrative Region, China (Ref No. T13-402/17-N).

Appendix A. Supplementary data

Supplementary data related to this article can be found at https://doi.org/10.1016/j.biomaterials.2017.12.007.

References

- [1] N.A. Mall, P.N. Chalmers, M. Moric, M.J. Tanaka, B.J. Cole, B.R. Bach Jr., G.A. Paletta Jr., Incidence and trends of anterior cruciate ligament reconstruction in the United States, Am. J. Sports Med. 42 (10) (2014) 2363–2370.
- [2] A. Ajuied, F. Wong, C. Smith, M. Norris, P. Earnshaw, D. Back, A. Davies, Anterior cruciate ligament injury and radiologic progression of knee osteoarthritis: a systematic review and meta-analysis, Am. J. Sports Med. 42 (9) (2014) 2242–2252.
- [3] C.L. Ardern, N.F. Taylor, J.A. Feller, K.E. Webster, Fifty-five per cent return to competitive sport following anterior cruciate ligament reconstruction surgery: an updated systematic review and meta-analysis including aspects of physical functioning and contextual factors, Br. J. Sports Med. 48 (21) (2014) 1543–1552.
- [4] Y.F. Chen, S. Lin, Y.X. Sun, X.H. Pan, L.B. Xiao, L.Y. Zou, K.W. Ho, G. Li, Translational potential of ginsenoside Rb1 in managing progression of osteoarthritis, J. Orthop. Translat. 6 (2016) 27–33.
- [5] G.V. Kamath, J.C. Redfern, P.E. Greis, R.T. Burks, Revision anterior cruciate ligament reconstruction, Am. J. Sports Med. 39 (1) (2011) 199–217.
- [6] G. Samitier, A.I. Marcano, E. Alentorn-Geli, R. Cugat, K.W. Farmer, M.W. Moser, Failure of anterior cruciate ligament reconstruction, Arch. Bone Joint Surg. 3 (4) (2015) 220–240.
- [7] P.P.Y. Lui, Y.W. Lee, T.Y. Mok, Y.C. Cheuk, K.M. Chan, Alendronate reduced peritunnel bone loss and enhanced tendon graft to bone tunnel healing in anterior cruciate ligament reconstruction, Eur. Cell. Mater. 25 (2013) 78–96.
- [8] D. Zhao, S. Huang, F. Lu, B. Wang, L. Yang, L. Qin, K. Yang, Y. Li, W. Li, W. Wang, S. Tian, X. Zhang, W. Gao, Z. Wang, Y. Zhang, X. Xie, J. Wang, J. Li, Vascularized bone grafting fixed by biodegradable magnesium screw for treating osteonecrosis of the femoral head. Biomaterials 81 (2016) 84–92.
- [9] J.W. Lee, H.S. Han, K.J. Han, J. Park, H. Jeon, M.R. Ok, H.K. Seok, J.P. Ahn, K.E. Lee, D.H. Lee, S.J. Yang, S.Y. Cho, P.R. Cha, H. Kwon, T.H. Nam, J.H. Han, H.J. Rho, K.S. Lee, Y.C. Kim, D. Mantovani, Long-term clinical study and multiscale analysis of in vivo biodegradation mechanism of Mg alloy, Proc. Natl. Acad. Sci. USA 113 (3) (2016) 716–721.
- [10] H. Windhagen, K. Radtke, A. Weizbauer, J. Diekmann, Y. Noll, U. Kreimeyer, R. Schavan, C. Stukenborg-Colsman, H. Waizy, Biodegradable magnesium-based screw clinically equivalent to titanium screw in hallux valgus surgery: short term results of the first prospective, randomized, controlled clinical pilot study, Biomed. Eng. Online 12 (2013) 62.
- [11] D.W. Zhao, F. Witte, F.Q. Lu, J.L. Wang, J.L. Li, L. Qin, Current status on clinical applications of magnesium-based orthopaedic implants: a review from clinical translational perspective, Biomaterials 112 (2017) 287–302.
- [12] Y. Zhang, J. Xu, Y.C. Ruan, M.K. Yu, M. O'Laughlin, H. Wise, D. Chen, L. Tian, D. Shi, J. Wang, S. Chen, J.Q. Feng, D.H. Chow, X. Xie, L. Zheng, L. Huang, S. Huang, K. Leung, N. Lu, L. Zhao, H. Li, D. Zhao, X. Guo, K. Chan, F. Witte, H.C. Chan, Y. Zheng, L. Qin, Implant-derived magnesium induces local neuronal production of CGRP to improve bone-fracture healing in rats, Nat. Med. 22 (10) (2016) 1160—1169.
- [13] D. Noviana, D. Paramitha, M.F. Ulum, H. Hermawan, The effect of hydrogen gas evolution of magnesium implant on the postimplantation mortality of rats, J. Orthop. Translat. 5 (2016) 9–15.
- [14] F. Witte, J. Fischer, J. Nellesen, H.A. Crostack, V. Kaese, A. Pisch, F. Beckmann, H. Windhagen, In vitro and in vivo corrosion measurements of magnesium alloys, Biomaterials 27 (7) (2006) 1013–1018.

- [15] F. Witte, V. Kaese, H. Haferkamp, E. Switzer, A. Meyer-Lindenberg, C.J. Wirth, H. Windhagen, In vivo corrosion of four magnesium alloys and the associated bone response, Biomaterials 26 (17) (2005) 3557–3563.
- [16] J. Kuhlmann, I. Bartsch, E. Willbold, S. Schuchardt, O. Holz, N. Hort, D. Hoche, W.R. Heineman, F. Witte, Fast escape of hydrogen from gas cavities around corroding magnesium implants, Acta Biomater. 9 (10) (2013) 8714–8721.
- [17] E. Willbold, X. Gu, D. Albert, K. Kalla, K. Bobe, M. Brauneis, C. Janning, J. Nellesen, W. Czayka, W. Tillmann, Y. Zheng, F. Witte, Effect of the addition of low rare earth elements (lanthanum, neodymium, cerium) on the biodegradation and biocompatibility of magnesium, Acta Biomater. 11 (2015) 554–562.
- [18] K. Bobe, E. Willbold, I. Morgenthal, O. Andersen, T. Studnitzky, J. Nellesen, W. Tillmann, C. Vogt, K. Vano, F. Witte, In vitro and in vivo evaluation of biodegradable, open-porous scaffolds made of sintered magnesium W4 short fibres, Acta Biomater. 9 (10) (2013) 8611–8623.
- [19] Y. Koo, H.B. Lee, Z. Dong, R. Kotoka, J. Sankar, N. Huang, Y. Yun, The effects of static and dynamic loading on biodegradable magnesium pins in vitro and in vivo, Sci. Rep. 7 (1) (2017) 14710.
- [20] J. Wang, Y. Jang, G. Wan, V. Giridharan, G.L. Song, Z. Xu, Y. Koo, P. Qi, J. Sankar, N. Huang, Y. Yun, Flow-induced corrosion of absorbable magnesium alloy: insitu and real-time electrochemical study, Corros. Sci. 104 (2016) 277–289.
- [21] S. Yoshizawa, A. Brown, A. Barchowsky, C. Sfeir, Magnesium ion stimulation of bone marrow stromal cells enhances osteogenic activity, simulating the effect of magnesium alloy degradation, Acta Biomater. 10 (6) (2014) 2834–2842.
- [22] P.F. Cheng, P. Han, C.L. Zhao, S.X. Zhang, X.N. Zhang, Y.M. Chai, Magnesium inference screw supports early graft incorporation with inhibition of graft degradation in anterior cruciate ligament reconstruction, Sci. Rep. UK 6 (2016)
- [23] J. Wang, J. Xu, W. Fu, W. Cheng, K. Chan, P.S. Yung, L. Qin, Biodegradable magnesium screws accelerate fibrous tissue mineralization at the tendonbone insertion in anterior cruciate ligament reconstruction model of rabbit, Sci. Rep. 7 (2017) 40369.
- [24] P.F. Cheng, P. Han, C.L. Zhao, S.X. Zhang, H.L. Wu, High-purity magnesium interference screws promote fibrocartilaginous entheses regeneration in the anterior cruciate ligament reconstruction rabbit model via accumulation of BMP-2 and VEGF, Biomaterials 81 (2016) 14–26.
- [25] J.L. Wang, J.K. Xu, B. Song, D.H. Chow, P.S.H. Yung, L. Qin, Magnesium (Mg) based interference screws developed for promoting tendon graft incorporation in bone tunnel in rabbits, Acta Biomater. 63 (2017) 393–410.
- [26] J.L. Wang, J. Tang, P. Zhang, Y.D. Li, J. Wang, Y.X. Lai, L. Qin, Surface modification of magnesium alloys developed for bioabsorbable orthopedic implants: a general review, J. Biomed. Mater. Res. B Appl. Biomater. 100B (6) (2012) 1691–1701.
- [27] T.T. Tang, L. Qin, Translational study of orthopaedic biomaterials and devices, J. Orthop. Translat. 5 (2016) 69–71.
- [28] Y.F. Zheng, X.N. Gu, F. Witte, Biodegradable metals, Mat. Sci. Eng. R 77 (2014) 1–34.
- [29] K.F. Farraro, K.E. Kim, S.L. Woo, J.R. Flowers, M.B. McCullough, Revolutionizing orthopaedic biomaterials: the potential of biodegradable and bioresorbable magnesium-based materials for functional tissue engineering, J. Biomech. 47 (9) (2014) 1979–1986.
- [30] X.N. Gu, X.H. Xie, N. Li, Y.F. Zheng, L. Qin, In vitro and in vivo studies on a Mg-Sr binary alloy system developed as a new kind of biodegradable metal, Acta Biomater. 8 (6) (2012) 2360–2374.
- [31] T. Dudev, C. Lim, Competition among Ca2+, Mg2+, and Na+ for model ion channel selectivity filters: determinants of ion selectivity, J. Phys. Chem. B 116 (35) (2012) 10703–10714.
- [32] F. Yang, D.Z. Yang, J. Tu, Q.X. Zheng, L.T. Cai, L.P. Wang, Strontium enhances osteogenic differentiation of mesenchymal stem cells and in vivo bone formation by activating Wnt/Catenin signaling, Stem Cell. 29 (6) (2011) 981–991
- [33] ASTM, Standard Test Methods for Tension Testing of Metallic Materials, 2004.
- [34] ASTM, Standard Practice for Laboratory Immersion Corrosion Testing of Metals. 1972.
- [35] C.R.M. Roesler, G.V. Salmoria, A.D.O. More, J.M. Vassoler, E.A. Fancello, Torsion test method for mechanical characterization of PLDLA 70/30 ACL interference screws, Polym. Test. 34 (2014) 34–41.
- [36] ISO, Metallic Materials-Wire-Simple Torsion Test, International Organization for Standardization, 2012.

- [37] ISO, 10993-12: Biological Evaluation of Medical Devices Part 12: Sample Preparation and Reference Materials, International Organization of Standards, 2012
- [38] J. Wang, F. Witte, T. Xi, Y. Zheng, K. Yang, Y. Yang, D. Zhao, J. Meng, Y. Li, W. Li, K. Chan, L. Qin, Recommendation for modifying current cytotoxicity testing standards for biodegradable magnesium-based materials, Acta Biomater. 21 (2015) 237–249.
- [39] A. Weiler, H.J. Windhagen, M.J. Raschke, A. Laumeyer, R.F.G. Hoffmann, Biodegradable interference screw fixation exhibits pull-out force and stiffness similar to titanium screws, Am. J. Sports Med. 26 (1) (1998) 119—128.
- [40] C.Y. Wen, L. Qin, K.M. Lee, K.M. Chan, Peri-graft bone mass and connectivity as predictors for the strength of tendon-to-bone attachment after anterior cruciate ligament reconstruction, Bone 45 (3) (2009) 545–552.
- [41] C. Maniatopoulos, A. Rodriguez, D.A. Deporter, A.H. Melcher, An improved method for preparing histological sections of metallic implants, Int. J. Oral Maxillofac, Implants 1 (1) (1986) 31–37.
- [42] H.F. Li, X.H. Xie, Y.F. Zheng, Y. Cong, F.Y. Zhou, K.J. Qiu, X. Wang, S.H. Chen, L. Huang, L. Tian, L. Qin, Development of biodegradable Zn-1X binary alloys with nutrient alloying elements Mg, Ca and Sr, Sci. Rep. 5 (2015) 10719.
- [43] M.X. Cheng, J.H. Chen, H.G. Yan, B. Su, Z.H. Yu, W.J. Xia, X.L. Gong, Effects of minor Sr addition on microstructure, mechanical and bio-corrosion properties of the Mg-5Zn based alloy system, J. Alloy. Comp. 691 (2017) 95-102
- [44] J.F. Nie, Effects of precipitate shape and orientation on dispersion strengthening in magnesium alloys, Scripta Mater. 48 (8) (2003) 1009–1015.
- [45] J.D. Robson, C. Paa-Rai, The interaction of grain refinement and ageing in magnesium-zinc-zirconium (ZK) alloys, Acta Mater. 95 (2015) 10–19.
- [46] J. Schatzker, F. Meutstege, W.D. Prieur, Manual of Internal Fixation in Small Animals, Springer- Verlag, Berlin, 1998.
- [47] C.C. Hsu, C.K. Chao, J.L. Wang, S.M. Hou, Y.T. Tsai, J. Lin, Increase of pullout strength of spinal pedicle screws with conical core: biomechanical tests and finite element analyses, J. Orthop. Res. 23 (4) (2005) 788–794.
- [48] A. Herrera, F. Martinez, D. Iglesias, J. Cegonino, E. Ibarz, L. Gracia, Fixation strength of biocomposite wedge interference screw in ACL reconstruction: effect of screw length and tunnel/screw ratio. a controlled laboratory study, BMC Muscoskel. Disord. 11 (2010) 139.
- [49] J. Nyland, R. Krupp, J. Greene, R. Bowles, R. Burden, D.N. Caborn, In situ comparison of varying composite tibial tunnel interference screws used for ACL soft tissue graft fixation, Knee 22 (6) (2015) 554–558.
- [50] P.P. Lui, Y.W. Lee, T.Y. Mok, Y.C. Cheuk, Peri-tunnel bone loss: does it affect early tendon graft to bone tunnel healing after ACL reconstruction? Knee Surg. Sports Traumatol. Arthrosc. 23 (3) (2015) 740–751.
- [51] P.P. Lui, Y.W. Lee, T.Y. Mok, Y.C. Cheuk, Local administration of alendronate reduced peri-tunnel bone loss and promoted graft-bone tunnel healing with minimal systemic effect on bone in contralateral knee, J. Orthop. Res. 31 (12) (2013) 1897–1906.
- [52] L.L. Wu, B.J.C. Luthringer, F. Feyerabend, A.F. Schilling, R. Willumeit, Effects of extracellular magnesium on the differentiation and function of human osteoclasts, Acta Biomater. 10 (6) (2014) 2843–2854.
- [53] D.P. Wornham, M.O. Hajjawi, I.R. Orriss, T.R. Arnett, Strontium potently inhibits mineralisation in bone-forming primary rat osteoblast cultures and reduces numbers of osteoclasts in mouse marrow cultures, Osteoporos. Int. 25 (10) (2014) 2477–2484.
- [54] H.F. Li, X.H. Xie, Y.F. Zheng, Y. Cong, F.Y. Zhou, K.J. Qiu, X. Wang, S.H. Chen, L. Huang, L. Tian, L. Qin, Development of biodegradable Zn-1X binary alloys with nutrient alloying elements Mg, Ca and Sr, Sci. Rep. UK 5 (2015).
- [55] Y. Yu, G. Jin, Y. Xue, D. Wang, X. Liu, J. Sun, Multifunctions of dual Zn/Mg ion co-implanted titanium on osteogenesis, angiogenesis and bacteria inhibition for dental implants, Acta Biomater. 49 (2017) 590–603.
- [56] D. Zhao, T. Wang, K. Nahan, X. Guo, Z. Zhang, Z. Dong, S. Chen, D.T. Chou, D. Hong, P.N. Kumta, W.R. Heineman, In vivo characterization of magnesium alloy biodegradation using electrochemical H2 monitoring, ICP-MS, and XPS, Acta Biomater. 50 (2017) 556–565.
- [57] B.L. Proffen, M. McElfresh, B.C. Fleming, M.M. Murray, A comparative anatomical study of the human knee and six animal species, Knee 19 (4) (2012) 493–499.
- [58] J. Tang, J. Wang, X. Xie, P. Zhang, Y. Lai, Y. Li, L. Qin, Surface coating reduces degradation rate of magnesium alloy developed for orthopaedic applications, J. Orthop. Translat. 1 (2013) 41–48.